American Mineralogist, Volume 83, pages 1188–1198, 1998

Semiquantitative determination of trans-vacant and cis-vacant 2:1 layers in illites and illite-smectites by thermal analysis and X-ray diffraction

VICTOR A. DRITS,[1] HOLGER LINDGREEN,[2,*] ALFRED L. SALYN,[1] ROBERT YLAGAN,[3] and DOUGLAS K. MCCARTY[4]

[1]Institute of Geology, Russian Academy of Science, Pyzhevsky per. D7, 109017 Moscow, Russia
[2]Clay Mineralogical Laboratory, Geological Survey of Denmark and Greenland, Thoravej 8, DK2400 Copenhagen NV, Denmark
[3]Exxon Production Research Co., P.O. Box 2189, Houston, Texas 77252-2189, U.S.A.
[4]Texaco Exploration and Production Technology Department, 3901 Briarpark, Houston, Texas 77042, U.S.A.

ABSTRACT

Interstratified illite-smectites (I/S) and illite-smectite-vermiculites (ISV) representing both hydrothermal and diagenetic transformations and having different degrees of structural order were investigated for cis-trans occupancy in the octahedral sheet by X-ray diffraction (XRD) and by differential thermal analysis (DTA) in combination with evolved water analysis (EWA) using an infrared detector. By XRD, the amounts of cis (w_{cv}) and trans (w_{tv}) vacant 2:1 layers were determined for the three-dimensionally ordered samples using both the WILDFIRE simulation program and calculations based on positions of the $11l$ and $11\bar{l}$ reflections. Based on the EWA curves, the I/S and ISV could be divided into three groups having (1) one strong and one or more weak EWA peaks; (2) two well-resolved peaks; and (3) a complex EWA curve. The amounts of cis- and trans-vacant sites were determined by peak fitting of the total dehydroxylation curve. The complex EWA curves were, however, in addition split into separate dehydroxylation processes during a step-heating technique. If the EWA peaks below and above 600 °C were attributed to trans vacant (tv) and cis vacant (cv) octahedra, respectively, the w_{cv} values determined by XRD and by EWA were in agreement. For the three-dimensionally ordered minerals, both XRD and EWA should be used, whereas the EWA method can be applied to the structurally disordered samples having no diagnostic $11l$ reflections. Accordingly, a combination of XRD and EWA for the determination of w_{cv} and w_{tv} supports an evaluation of the mechanism of illitization in various geological environments. Thus, significant changes in w_{cv} and w_{tv} during illitization are likely due to a dissolution-precipation, whereas almost constant values indicate a solid-state transformation.

INTRODUCTION

Interstratified illite-smectite (I/S) is present in different geological environments, and the structure (amount of illite interlayers and ordering of the interlayer types) is an indicator of the degree of transformation both during burial diagenesis and hydrothermal activity (Burst 1969; Shutov et al. 1969; Hower et al. 1976; Bethke and Altaner 1986; Nadeau and Bain 1986; Inoue et al. 1988; Eberl 1993).

Characterization of I/S and the mechanisms of I/S formation at different stages of postsedimentary and hydrothermal alteration of rocks have been extensively studied (Shutov et al. 1969; Hower et al. 1976; Pevear et al. 1980; Reynolds 1980; Środoń 1980, 1984). Until recently, mainly the mixed-layering of the I/S structure has been studied through investigation of basal reflections by X-ray diffraction (XRD) and through attempts to image the distribution of illite and smectite interlayers using high resolution transmission electron microscopy (Ahn and Peacor 1986a, 1986b, 1989; Bell 1986; Klimentidis and MacKinnon 1986; Hansen and Lindgreen 1987, 1989; Guthrie and Veblen 1989; Ahn and Buseck 1990; Veblen et al. 1990; Lindgreen and Hansen 1991; Środoń et al. 1992; Šucha et al. 1996). Furthermore, electron microscopy has been used to determine shape and thickness of particles (Nadeau et al. 1984, 1985; Inoue et al. 1987; Lanson and Champion 1991; Šucha et al. 1992; Inoue and Kitagawa 1994).

Tsipursky and Drits (1984) showed that in the 2:1 layers of montmorillonite, as a rule, one of two symmetrically independent cis-octahedra is vacant, whereas illites normally have trans-vacant (tv) 2:1 layers. Accordingly, a formation of illite 2:1 layers from smectite 2:1 layers should lead to an increase in proportion of tv 2:1 layers. Investigations of the change in amount of cis-vacant (cv) and tv 2:1 layers in I/S during transformations should accordingly be important for understanding the mechanisms and dynamics of this process. For example, Drits

* E-mail: HL@geus.dk.

0003–004X/98/1112–1188$05.00

(1987) showed, that during diagenesis of pyroclastic rocks in the Karaganda Basin, Kazakhstan, transformation of I/S is accompanied not only by increasing the illite interlayers and in short-range layer ordering, but also by a change in distribution of octahedral cations within the 2:1 layers. Reynolds (1993) and McCarty and Reynolds (1995) showed that fundamental illite particles in I/S samples from the Appalachian basin and neighboring areas consist of randomly interstratified tv and cv 2:1 layers. Drits et al. (1996) studied the transformation of I/S samples from Dolná Ves hydrothermal deposits and found also that the I/S structure consisted of interstratified tv and cv 2:1 layers. Similar results were obtained by Ylagan et al. (1996).

Two methods are presently used to determine the proportion of tv and cv 2:1 layers in I/S by XRD. The first method is based on simulation of experimental XRD powder patterns (Drits et al. 1984; Reynolds 1993). The second is a semiquantitative calculation of the amount of interstratified tv and cv 2:1 layers from the d(11*l*) values alone (Drits and McCarty 1996). Neither method can be applied properly to I/S having XRD patterns with no modulations of diffracted intensities in the diagnostic region containing 11*l* and 02*l* reflections. However, I/S having highly disordered structures are widely spread in the nature especially in shales.

Drits et al. (1995) showed that smectites and illites consisting of cv 2:1 layers have dehydroxylation temperatures 100 to 200 °C higher than those consisting of tv 2:1 layers. These results explain differences in the DTA curves of illites. For instance, Drits et al. (1995) showed that "abnormal" illite described by Mackenzie (1957) consists of cv 2:1 layers. It is well known that differential thermal DTA curves for some of the dioctahedral smectites, illites, and I/S have a doublet between 500 and 700 °C probably due to two endothermic reactions (Mackenzie 1957; Grim 1968). Drits et al. (1995) suggested that the size of each of these endothermal peaks probably reflected the proportions of tv and cv layers. The main aim of this paper is to test this hypothesis through an investigation of illites, I/S, and illite-smectite-vermiculites (ISV) by both XRD and thermal analysis.

Materials and methods

Samples

Potassium, iron, and magnesium contents per $O_{10}(OH)_2$ of the samples are given in Table 1. Four different localities were used: rhyolitic volcanoclastics transformed through hydrothermal activity from Ponza Island, Italy (Ylagan 1996; Ylagan et al. 1996) and Dolná Ves, Slovakia (Šucha et al. 1992; Drits et al. 1996); upper Jurassic oil source rock shales, transformed through burial diagenesis from the North Sea and onshore Denmark (Hansen and Lindgreen 1989; Lindgreen and Hansen 1991; Drits et al. 1997); and K-bentonites from the Appalachian Basin and neighboring areas probably transformed by migrating fluids (McCarty and Reynolds 1995).

Table 1. Sample localities and structural parameters

Sample	Location	w_s*	*R*†	Size (μm)	K‡	Fe‡	Mg‡
Canada 35	Ottawa	0.21	2.5	<1	0.49	0.12	0.26
Canada 30	Ottawa	0.13	2.5	<1	0.67	0.08	0.42
GA:DD	Millbrig., GA	0.14	3	<0.5	0.63	0.36	0.44
NAS-1	Nasset, IA	0.15	3	<1	0.67	0.13	0.64
GAFL 1-1	Deicke, GA	0.09	3	<0.5	0.51	0.37	0.36
WT5B	Tioga, NY	0.13	3	<0.5			
93-6-11C	Ponza Island	0.68	0	<0.1	0.20	0.19	0.34
93-6-9C	"	0.28	1.36	<0.1	0.44	0.24	0.17
93-6-8Q	"	0.48	0.5	<0.1	0.33	0.18	0.39
93-6-8N	"	0.10	R3	<0.5	0.56	0.15	0.18
93-6-9Q	"	0.41	1	<0.1	0.35	0.25	0.32
93-6-9L	"	0.21	1.5	<0.5	0.57	0.03	0.17
93-6-8C	"	1.00	0	<0.5	0.02	0.17	0.43
93-6-8W	"	0.00	3	<0.1			
93-6-16T	"	0.07	3	<0.5	0.69	0.06	0.28
93-6-10A	"	0.00	3	<0.5	0.68	0.04	0.27
1602	Dolná Ves	0.14	3	<1	0.56	0.05	0.28
1603	"	0.08	3	<1	0.61	0.14	0.16
1617	"	0.40	1	<1	0.46	0.08	0.19
2204	"	0.40	1	<1	0.49	0.14	0.13
95	Denmark	0.70	1		0.31	0.47	0.29
x3	North Sea	0.80	1		0.33	0.23	0.33
x18	"	0.90	1		0.52	0.19	0.21
89	"	0.84	1		0.40	0.16	0.14

* Amount of smectite.
† Short-range ordering factor.
‡ Moles per $O_{10}(OH)_2$.

Pretreatment

The I/S was separated from volcanic rocks by gentle crushing, disaggregation in distilled water with an ultrasonic probe, and separation of different size fractions by centrifugation. The fractions <0.1 μm or <0.5 μm of I/S from Ponza Island and the <1 μm size fraction of the I/S from Dolná Ves (Table 1) were investigated. Because of the complex mineralogical composition of the samples of the North Sea shales, the ISV had to be separated by a special methodology. These samples were treated for removal of organic matter and Fe- and Al-oxides and the finest size fractions consisting of ISV together with small amounts of kaolinite-illite-vermiculite were isolated by centrifugation as described by Hansen and Lindgreen (1989). The particles of this fraction are according to scanning probe microscopy predominantly <500 Å in diameter and <100 Å in thickness (Lindgreen et al. 1992).

X-ray diffraction

I/S and ISV expandability, w_s, and the short-range ordering factor, *R*, (Table 1) were determined from the XRD patterns of the glycolated and oriented specimens using the computer programs developed by Drits and Sakharov (1976) and by Reynolds (1985). Contents of tv (w_{tv}) and cv (w_{cv}) layers were determined by powder XRD by two methods. The first one based on simulation of XRD patterns for different models using the computer program WILDFIRE (Reynolds 1993) was applied to determine the w_{cv} values for the I/S samples from Appalachian Basin (McCarty and Reynolds 1995) and Ponza Island (Ylagan 1996). Simulated and the experimental XRD patterns agree (Fig. 1) for samples Canada 30 and Canada 35. The

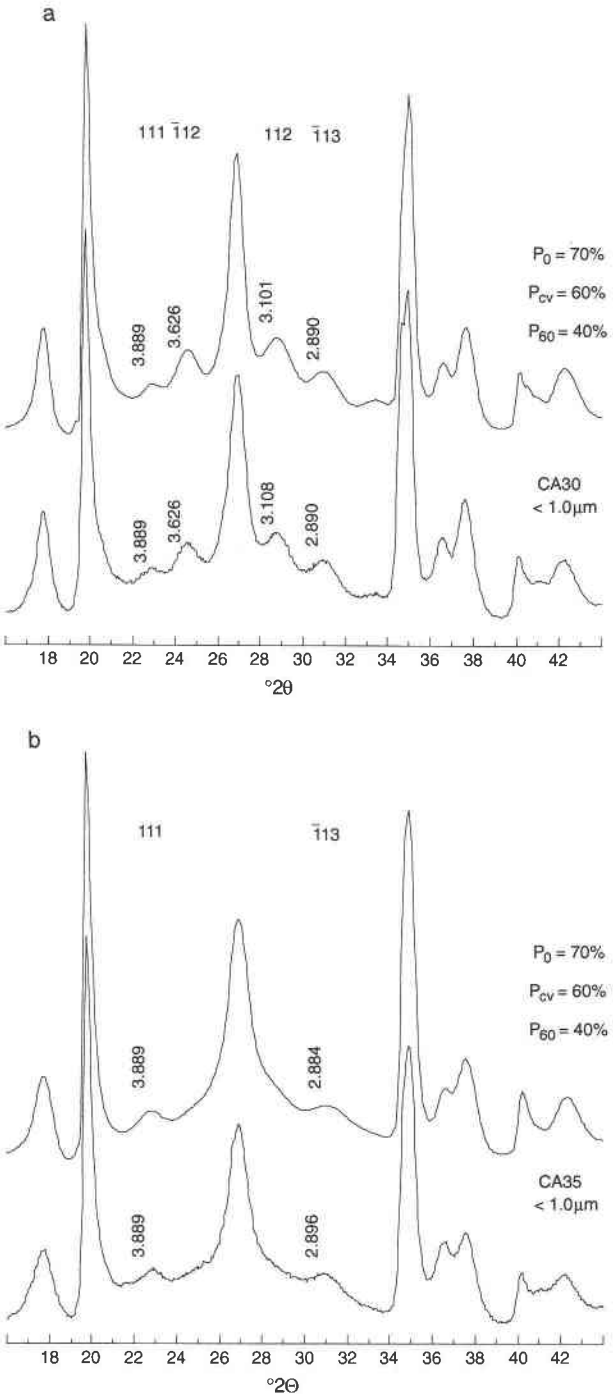

FIGURE 1. Calculated (top) and experimental (bottom) diffraction patterns. Cu$K\alpha$-radiation. The calculated pattern is for one phase having the parameters shown. (**a**) Canada 30. (**b**) Canada 35.

second method developed by Drits and McCarty (1996) was applied to I/S samples whose XRD patterns contained noticeable intensity modulations corresponding to 11*l* reflections.

Thermal analysis

EWA curves. A Stanton Redcroft DTA 673-674 with gas outlet to non-dispersive infrared H_2O and CO_2 detectors was used to determine quantitatively the amount of structural water released during heating (evolved water analysis, EWA). Detailed description of this combined apparatus was given by Morgan (1977). The main advantage of this technique is that the loss of hydroxyls is recorded separately and that the amount of structural water released during dehydroxylation can be determined quantitatively and with high sensitivity.

Sodium-saturated samples were heated at 5 °C/min in a gas flow of 300 ml N_2 per min. To separate dehydration and dehydroxylation processes, the samples were heated first to 200 °C and the temperature was then kept constant until the water release stopped. The samples were next heated further to 1000 °C at 5 °C/min.

Numerical decomposition of EWA curves. The EWA curve profile was fit with individual maxima having different temperatures. The positions and number of the main peaks were determined, first visually and then through the minimization procedure. The computer program developed for this purpose minimizes the difference between the experimental profile and the profile synthesized after summation of individual peaks. Each individual maximum was a combination of two Gaussian functions. One function describes the upper part of the peak profile with steep slopes (the upper Gaussian) and the other (the lower Gaussian), which was twice as wide, describes the lower, less steep part of the peak. Peak position, width at half height of the "upper" Gaussian and relative contribution of the "lower" Gaussian to the total peak area were used as variable parameters of each peak. However, only for one of the individual peaks were two Gaussian functions needed. The quality of the approximation was estimated by the *R* factor, which is the relative difference between the observed and the synthesized profiles (see also Drits et al. 1993).

Stepwise heating. This technique was applied for samples having complex dehydroxylation curves. After equilibration at 200 °C, the temperature was again increased at a rate of 5 °C/min. When the temperature of the first shoulder or peak observed previously in the continuous dehydroxylation curve was recorded, the temperature was kept constant until the EWA curve had dropped to base level, and then the heating was resumed. If the dehydroxylation during this heating stage showed a maximum, the next constant heating stage was introduced. This process was repeated to 1000 °C depending on the maxima observed during the analysis.

RESULTS AND DISCUSSION

X-ray diffraction

A wide range of w_{cv} was obtained by both methods (Table 2). Generally, for each of these samples the relative difference between the w_{cv} values does not exceed 20%. One exception is GAFL 1-1 for which the w_{cv} de-

TABLE 2. Proportions of cis-vacant layers (w_{cv}) from EWA and XRD

Sample	EWA	XRD			Difference‡	Step§
		Sim*	Eqs†	Ave		
Canada 35	51	70	56	63	12	51
Canada 30	58	60	59	60	2	
GA:DD	66	55	51	53	13	41
NAS-1	39	34	35	34	5	
GAFL-1	17	40	23	31.5	14	32
WT5B	76	98	70	84	8	78
93-6-11C	46	55	—	55	9	
93-6-9C	23	30	28	29	6	
93-6-8Q	71	70	—	70	1	
93-6-8N	37	33	43	38	1	
93-6-9Q	57	60	—	60	3	
93-6-9L	77	75	78	76	1	
93-6-8C	78	85	—	85	7	
93-6-8W	00	00	8	4	4	
93-6-16T	34	25	21	23	11	
93-6-10A	26	20	23	21.5	4	11
1602	70	—	65	65	5	
1603	53	—	—	—		
1617	80	—	90	90	10	
2204	64	—	85	85	21	
95	8	—	—	—		
x3	22					15?
x18	8	—	—	—		
89	22					4

* Using WILDFIRE simulation (Reynolds 1993).
† Using the method of Drits and McCarty (1996).
‡ w_{cv}(EWA) − w_{cv}(XRD).
§ From Step EWA analysis.

termined by simulation of the experimental XRD pattern (40%) is almost twice the w_{cv} determined by the technique of Drits and McCarty (1996). Drits and McCarty (1996) obtained for natural I/S samples similar levels of accuracy of w_{cv} through determination by WILDFIRE and by the method of Drits and McCarty (1996). Therefore, the average of the two w_{cv} values obtained for the same sample by both techniques should be the most reliable value (Table 2).

Dehydroxylation and octahedral site occupancy

Dehydroxylation patterns. According to the model of Drits et al. (1995), cv and tv 2:1 layers should have dehydroxylation temperatures above and below 600 °C, respectively. From the EWA curves, the I/S and ISV can be divided into three groups. The first group includes the I/S samples having one strong and one or more weak endothermal peaks (Fig. 2). Six samples (1617, 93-6-9L, 1602, 93-6-8C, NAS-1, and WT5B) have the main dehydroxylation reaction near 700 °C. Thus, cv 2:1 layers predominate in these samples. In contrast, samples 95, 92, x18, and x3 have the main dehydroxylation temperature T_{dh} below 550 °C and consist thus mainly of tv 2:1 layers.

The second group of samples (93-6-11C, -9C, -8Q, -16T, 2204, 93-6-8N, and -8W) has two well-resolved peaks, corresponding to two main endothermic reactions between 500 and 700 °C (Fig. 3). The ratio between the peak areas probably reflects the ratio between tv and cv 2:1 layers. For example, the EWA curve of sample 93-6-11C (Fig. 3a) has two peaks of almost equal size probably due to similar amounts of cv and tv layers in the sample. In the EWA curve of sample 93-6-8Q (Fig. 3b), the peak at ~670 °C is stronger than the peak at ~500 °C, and the

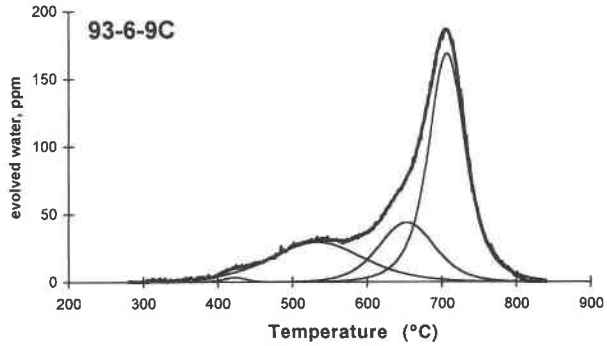

FIGURE 2. Experimental and simulated evolved water curve for sample 93-6-9L. Heating rate 5 °C/min.

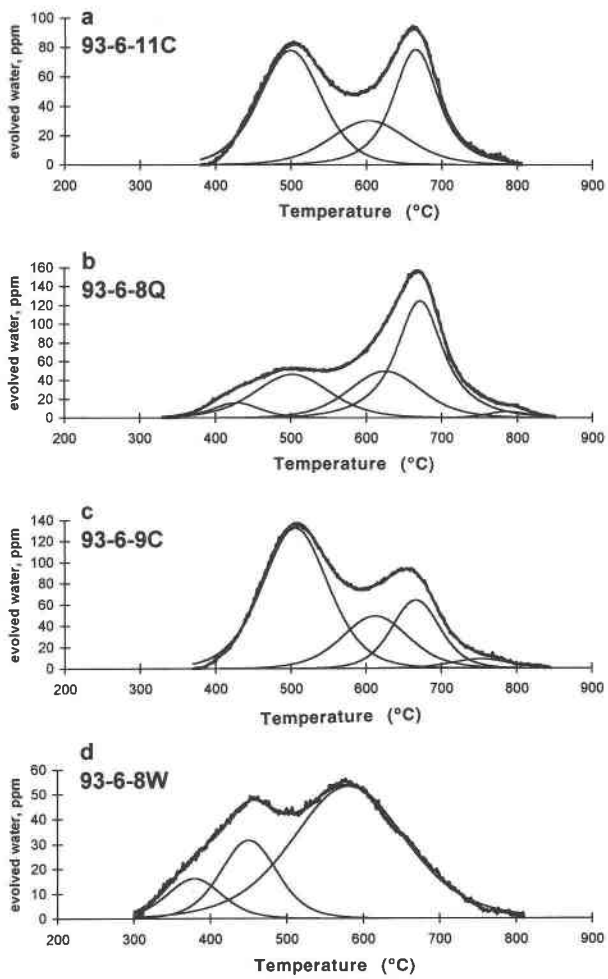

FIGURE 3. Experimental and simulated evolved water curves. Heating rate 5 °C/min.

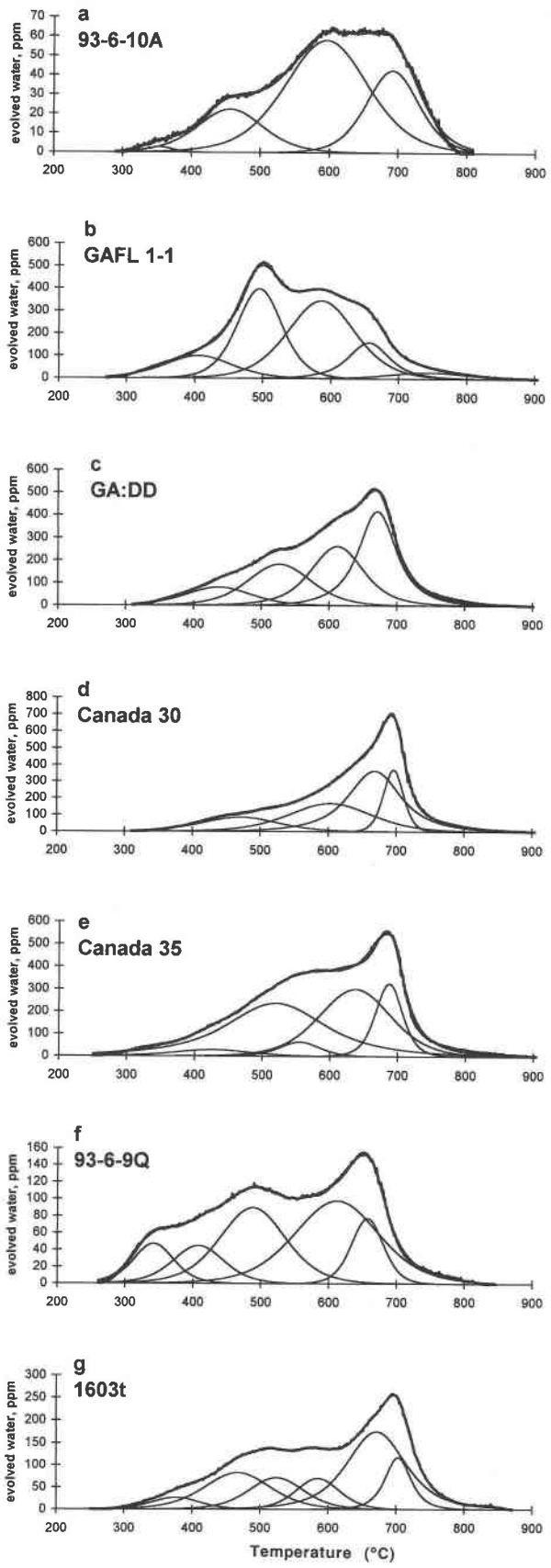

FIGURE 4. Experimental and simulated evolved water curves. Heating rate 5 °C/min.

→

amount of cv layers is larger than the amount of tv layers. In contrast, sample 93-6-9C has a larger peak at 500 °C than at 660 °C indicating that the amount of tv layers is larger (Fig. 3c). In sample 93-6-8W both peaks are located at temperatures <600 °C and the sample probably consists of only tv 2:1 layers (Fig. 3d).

The third group of samples has poorly resolved peaks (Fig. 4). However, even for these samples, amounts of cv and tv 2:1 layers can be determined. For example, the EWA curve of sample 93-6-10A has three poorly resolved peaks at ~450, ~590, and ~680 °C (Fig. 4a). The sum of the areas of the first two peaks appears to be larger than that of the last peak at ~680 °C. Accordingly, in sample 10A (Fig. 4a) as well as in GAFL 1-1 (Fig. 4b), the amount of tv 2:1 layers should be larger than of cv 2:1 layers, in samples GA:DD and Canada 30 the amount of cv layers is probably larger than of tv layers (Figs. 4c and 4d), whereas the samples 93-6-9Q and 1603 have equal proportions of both layer types (Figs. 4f and 4g).

Numerical decomposition of dehydroxylation curves. One or two individual peaks had T_{dh} >600 °C (Figs. 2 to 4). The peak having the highest dehydroxylation temperature at 650–700 °C could usually be observed visually, whereas the presence or absence of a second peak having lower dehydroxylation temperature (620–660 °C) was established during the decomposition procedure. From one to three peaks had T_{dh} <600 °C (Figs. 2–4). Their position could usually be observed visually and peak positions were refined during the minimization procedure. Temperatures and areas of individual decomposed peaks providing the best agreement between the observed and the synthesized EWA curves are given in Table 3.

Analytical step-heating decomposition. Eight I/S samples of group three having complex dehydroxylation patterns were analyzed by the step-heating technique. The curves are shown in Figure 5 and the peak areas and temperatures in Table 4. The complex monotonically increase heating curves of these samples were split into two almost symmetrical peaks in the region 500–610 °C and 640–710 °C. In some cases, one symmetrical peak occurred at 450 °C. The peaks are symmetrical despite the fact that the low-temperature half of the peak corresponds to heating at 5 °C/min and the high-temperature half of the peak to continued increase in temperature or alternatively to keeping temperature constant at the value for the peak or shoulder. This symmetry indicates that the peaks actually are due to single dehydroxylation processes. The splitting of the complex curves of group three samples into two separate peaks by step heating demonstrates similarity to the dehydroxylation processes of group two samples having two well-defined peaks.

TABLE 3. Numerical decomposition of EWA curves

Sample	EWA dehydroxylation peaks									
	°C	Area	°C	Area	°C	Area	°C	Area	°C	Area
Canada 35	427	3.6	520	41.4	555	4.2	637	35.8	687	15.0
Canada 30	470	13.2	603	28.4	668	43.2	696	15.2		
GA:DD	437	10.7	527	23.7	612	29.3	670	36.3		
NAS-1	468	13.3	584	47.3	643	32.1	761	7.3		
GAFL 1-1	405	11.6	495	31.2	586	40.7	656	12.6	744	3.9
WT5B	518	13.5	590	10.4	642	15.5	714	60.7		
93-6-11C	499	43.8	603	21.2	665	34.9				
93-6-9C	506	55.9	612	21.0	660	19.9	752	3.2		
93-6-8Q	428	5.1	502	23.7	625	24.4	671	45.0	787	1.8
93-6-8N	462	15.7	552	47.2	652	21.1	685	16.0		
93-6-9Q	408	12.2	490	31.2	612	43.5	656	13.1		
93-6-9L	533	23.3	653	20.8	708	55.9				
93-6-8C	435	21.6	624	38.9	675	39.4				
93-6-8W	450	23.1	580	76.9						
93-6-16T	440	6.4	570	59.6	640	4.5	701	29.5		
93-6-10A	456	17.2	596	56.6	692	26.2				
1602	516	29.5	660	22.3	709	48.2				
1603	467	20.7	524	14.8	585	11.5	676	40.8	703	12.2
1617	505	20.5	682	79.5						
2204	503	38.6	645	25.1	690	27.7	800	8.5		
95	466	38.1	510	30.3	578	23.2	681	8.4		
x3	527	76.3	634	13.3	727	10.4				
x18	506	51.6	561	45.1	744	3.3				
89	462	35.4	554	42.1	632	10.7	684	11.8		

Cis layer content determined by peak fitting. Table 2 contains w_{cv} values obtained by assuming that the ratio between areas of peaks with temperatures higher and lower than 600 °C corresponds to the ratio between cv and tv 2:1 layers, respectively. However, after decomposition, the EWA curves for samples Canada 30 and 93-6-11C have a peak with $T_{dh} \approx 600$ °C (Figs. 4d and 3a), which may be due to dehydroxylation of tv as well as of cv layers. For 93-6-11C having a large proportion of smectite layers ($w_S = 0.68$), we have assigned the area of this peak to cv layers and for Canada 30 having a small proportion of smectite layers ($w_S = 0.13$) to tv layers, because these assignments are in agreement with the XRD data and fits the hypothesis that the higher the w_I, w_{cv}, and R values, the higher the dehydroxylation temperatures of tv layers, see later.

For 15 samples the difference between w_{cv} determined by the XRD or EWA methods does not exceed 10% (averaged value is 4.5%). For four samples (Canada 35, GA:DD, GAFL 1-1, and 93-6-16T) these values vary from 11 to 14%, and only for sample 2204 does this value increase to 21% (Table 2).

For an I/S sample containing a significant amount of rotational stacking faults, a reliable determination of tv and cv layers by simulation of XRD patterns is not always possible because the 11*l* reflections are very broad and weak or simply absent. For such samples, the combination of results obtained by the thermal and the XRD methods may be very useful. For example, McCarty and Reynolds (1995) simulated the XRD pattern of sample Canada 35 and found that this sample should contain 95% of cv layers interstratified with 5% of tv layers. However, the EWA curve of this sample shows that a considerable amount of OH groups was lost at temperatures much lower than 600 °C (Fig. 4e), and the sample should therefore contain a significant amount of tv layers. A satisfactory agreement between experimental and calculated XRD patterns is shown for a new model that contains a physical mixture of crystals consisting either of tv layers (30%) or of cv layers (70%), each with different degree of rotational stacking faults (Fig. 6).

Cis layer content from step heating. This technique was applied to the samples of group three because of their complicated EWA curves. For sample 93-6-10A, the second peak in the step heating EWA curve (Fig. 5a) is assigned to tv layers despite the fact that its peak temperature (610 °C) is slightly above the upper limit of 600 °C used for tv 2:1 layer determination. This sample differs from the others by absence of expandable layers and a very high structural ordering. In addition to 1M, it contains 15% of the $2M_1$ modification. Probably, these features provide the increase of T_{dh} for tv layers. As discussed below, this agrees well with the hypothesis that the dehydroxylation temperature of tv layers depends on their content and distribution in this sample. Only for two samples, Canada 35 and WT5B, are the w_{cv} values calculated from the two EWA techniques similar (Figs. 5d and 5f, Table 2). For samples GA:DD and GAFL 1-1, the w_{cv} values obtained by step heating are close to the average w_{cv} values determined by XRD but different from those determined by numerical EWA decomposition (Table 2). In contrast, for sample 93-6-10A, the step heating w_{cv} value is different from the numerical EWA decomposition and the XRD w_{cv} values, which on the other hand are close to each other (Table 2). These data lead to two conclusions. First, for complex EWA curves a combination of the two EWA techniques are necessary to obtain a reliable estimate of w_{cv} and w_{tv}

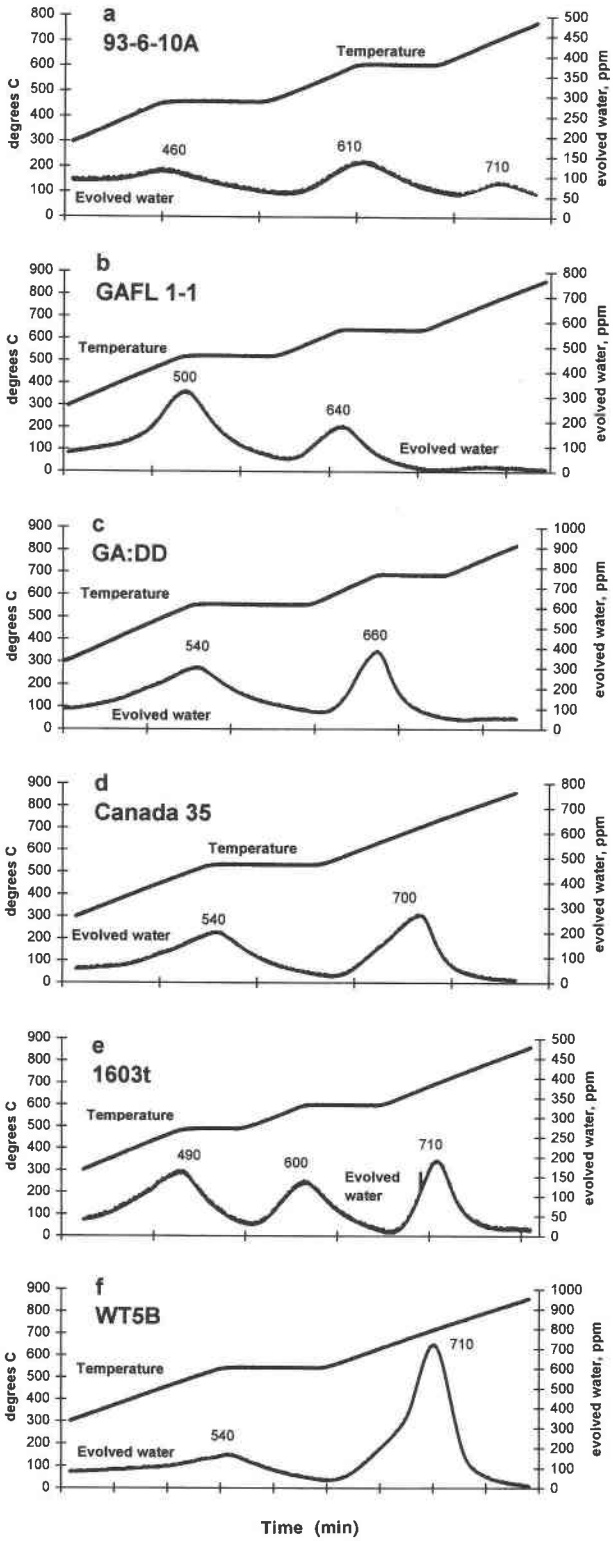

FIGURE 5. Evolved water curves and recorded temperature for step-wise heating. Heating at 5 °C/min. interrupted by constant-temperature intervals.

TABLE 4. EWA analysis, stepwise heating

Sample	T (°C)	Area (%)	T (°C)	Area (%)	T (°C)	Area (%)
Canada 35	540	49	700	51		
GA:DD	540	59	660	41		
GAFL 1-1	500	68	640	32		
WT5B	540	22	710	78		
93-6-10A	460	31	610	58	710	11
1603	490	41	600	28	700	31
x3	510	85	600	15		
89	500	96	620	4		

(Table 2). Second, for I/S samples having broad, weak, or absent diagnostic 11*l* reflections and complex EWA curve profiles, the errors of the different techniques are similar. Therefore, a combination of diffraction and thermal analysis is optimal for investigation of such poorly crystallized I/S samples.

EWA curves for the North Sea samples

The North Sea samples were not studied by XRD because their XRD patterns lacked diagnostic reflections. EWA curves have only one strong and broad dehydroxylation maximum at 510–550 °C (Fig. 7). Numerical decomposition shows that tv layers dominate in these samples. However, for samples x3 and 89 this technique shows 24 and 22% of cv layers, respectively (Figs. 7a and 7c). The step-heating technique reveals the last high-temperature maximum at 600 °C and area 15% for sample x3 (Fig. 8a) and 640 °C and 4% for sample 89 (Fig. 8b). Formally, the w_{cv} values obtained by the two EWA techniques for sample x3 are compatible (Table 2) but the shift in peak positions from 636 °C and 768 °C in the numerical EWA decomposition (Fig. 7a) to 600 °C in the step heating EWA curve (Fig. 8a) makes the assignment

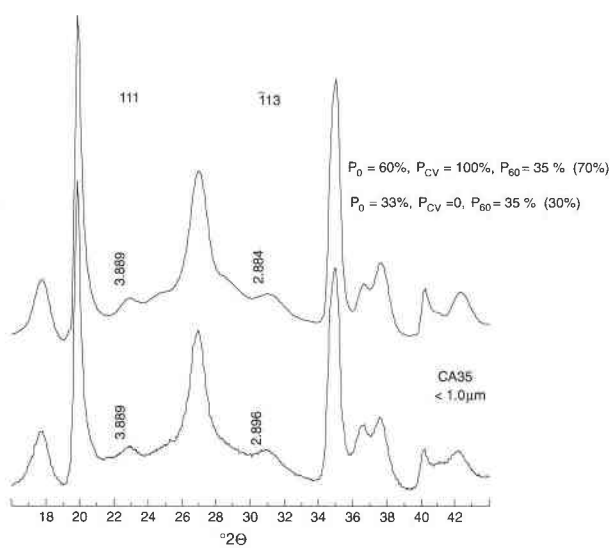

FIGURE 6. Calculated (top) and experimental (bottom) diffraction patterns for the sample Canada 35. Cu*K*α-radiation. The calculated pattern is for two phases having the parameters shown.

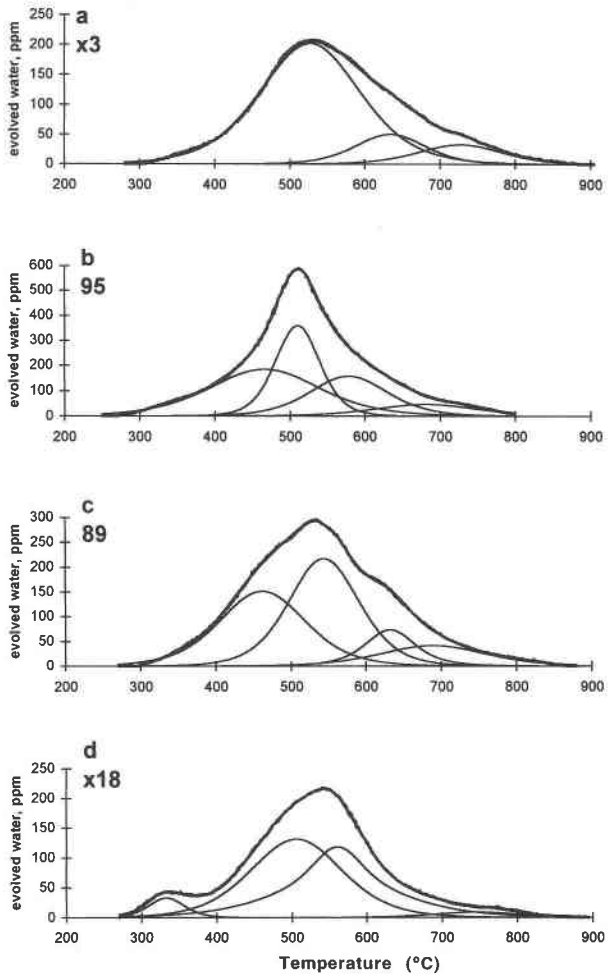

FIGURE 7. Experimental and simulated evolved water curves. Heating rate 5 °C/min.

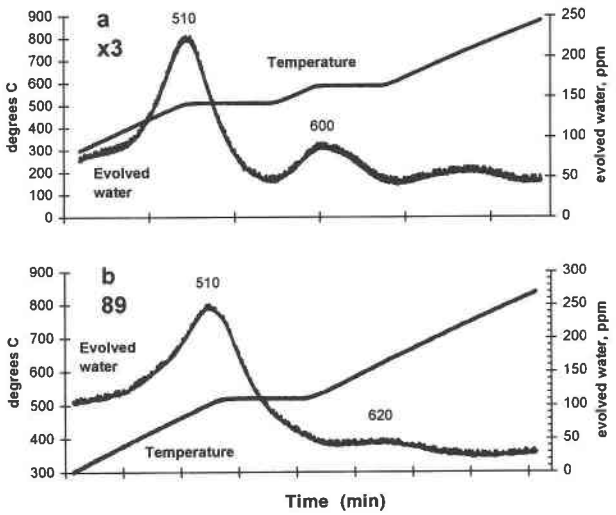

FIGURE 8. Evolved water curves and recorded temperature for step-wise heating. Heating at 5 °C/min. interrupted by constant-temperature intervals.

of this peak to cv layers uncertain. Moreover, as in the case of sample 93-6-10A, this peak may be assigned to tv layers. For sample 89, the last high-temperature maxima in both decompositions have temperatures significantly higher than 600 °C and are thus due to cv layers. However, for this sample the w_{cv} value equal to 4% in the step-heating analysis is significantly lower than the w_{cv} value obtained by the numerical EWA decomposition. Therefore, the cv layer content in the North Sea samples probably does not exceed 10%.

The high-temperature shoulders in the EWA curves of samples dominated by tv layers may be due to heterogeneous dehydroxylation (Guggenheim 1990). In aluminous fine-grained 2:1 phyllosilicates, a dehydroxylated octahedral tv sheet is similar to the original tv sheet, but contains fivefold-coordinated cations instead of Al octahedra. Based on Pauling's rules, Guggenheim (1990) assumed that during partial dehydroxylation at relatively low temperature the formation of pentagonal prisms occupied by Al increases the Al-OH bond strength in the Al octahedra having one or two shared edges with the pentagonal prisms. These more strongly bonded OH groups then require additional thermal energy for the dehydroxylation process to proceed. Each step of dehydroxylation results in an increasing proportion of pentagonal polyhedra, which further increases the Al-OH bond strength, and more thermal energy for the next step of the reaction is then required. In EWA curves, this process may lead to both increased peak width and high-temperature asymmetry and probably is responsible for the overestimation of the w_{cv} by numerical EWA decomposition. Therefore, when I/S or illite samples have a highly disordered structure and badly resolved EWA curves application of the step-heating technique may be especially useful for determination of the w_{cv} and w_{tv}.

Relationship between the dehydroxylation temperature and layer type content and distribution

Our results suggest that the dehydroxylation temperature of tv 2:1 layers depends on proportion and ordering of illite tv layers in I/S samples, such that the higher the w_I and R values, the higher is the dehydroxylation temperature of tv layers. For example, samples 93-6-8W, -10A, -16T, and -8N have a high proportion of tv illite layers ($0.62 < w_{tv} < 1$), low expandability ($w_S < 0.10$) and $R = 3$ (Table 1) and the main dehydroxylation of tv layers took place near 580 °C (Fig. 4a). In contrast, samples 93-6-8C, -8Q, -9Q, and -11C have significantly less tv layers and illite layers with $R \leq 1$ and $0.22 < w_{tv} < 0.45$, $w_S > 0.40$, and dehydroxylation temperatures of EWA peaks range from 440 to 500 °C (Figs. 3a, 3b, and 4f). Samples x18, 93-6-9C, and -9L have $0.20 < w_S < 0.40$, $0.7 < w_{tv} < 0.9$, and $1 \leq R < 2$ and the main dehydroxylation temperature of tv layers near 510–550 °C (Figs. 7d, 2, and 3c).

Similar regularities are observed for the dehydroxylation temperature of cv 2:1 layers. Samples 93-6-9L,

WT5B, and 1602 have a high proportion of cv illite layers ($0.70 < w_{cv} < 0.84$), low expandability ($w_s < 0.14$) and $R = 3$ (Figs. 2 and 5f) and the main dehydroxylation of cv layers near 710–715 °C. In contrast, samples 93-6-8C and -8Q, which also have a high proportion of cv layers (0.85 and 0.71, respectively) differ from 93-6-9L, WT5B, and 1602 in having a random layer distribution and a high content of smectite layers (1.0 and 0.48, respectively) and their decomposed EWA curves have two high-temperature maxima at 625 and 675 °C, respectively (Fig. 3b).

Changes in octahedral vacancies during I/S and ISV transformations

Determination of cv and tv layers by diffraction and thermal techniques may clarify the mechanism of illitization in a variety of geological environments. The Ordovician K-bentonites from the U.S.A. have different cv layer proportions with no correlation to the amount of illite layers. McCarty and Reynolds (1995) concluded that the content of tv and cv layers in these I/S samples is dependent on their chemical composition and not on expandability. Contrarily to this, during burial diagenesis of pyroclastic rocks in the Karaganda Basin illitization was accompanied by a change in the cv/tv ratio for the 2:1 layers (Drits 1987). During hydrothermal transformation of rhyolitic volcanoclastics, the amount of cv layers decreased with increase of illite layers in I/S samples (Drits et al. 1996). Accordingly, the reaction was a solid-phase transformation of smectite to illite layers up to 50% illite layers at which stage all 2:1 layers have cv sites, whereas the further increase in amount of illite layers up to 90% was a dissolution-reprecipitation process during which cv layers were replaced by tv 2:1 layers. Similar regularities are observed for hydrothermally altered I/S samples from Ponza Island (Ylagan 1996). For our rhyolitic volcanoclastics, generally w_{cv} increases with increasing expandability (w_s) and with decreasing content of K per $O_{10}(OH)_2$ (Figs. 9a and 9b, respectively), the only deviation from this trend being sample 93-6-9L.

Deconinck and Chamley (1995) found two types of smectitic minerals in the Upper Cretaceous chalks of northern France. The first type contains 65–95% smectite layers, has DTA dehydroxylation peaks at ~500 °C and was assumed to originate from continental weathering in a warm, seasonable humid climate. The second type contains 90–100% smectite layers, has a dehydroxylation peak at 600–700 °C and was interpreted to be authigenic. From the results of the present investigation, the first type must have tv and the second type cv 2:1 layers. The tv 2:1 layers in the I/S having different expandability and assumed to have formed during continental weathering may be due to that these I/S have formed from weathering of mica or illite, which is usually tv, whereas the presumably authigenic I/S have the cv 2:1 layers normally found in smectite (Tsipursky and Drits 1984).

The North Sea ISV consist mainly of tv layers but may have a small proportion of cv layers. This proportion does not correlate with the amount of illite layers or the degree of burial diagenesis. Hansen and Lindgreen (1989) and Lindgreen (1991) suggested that the North Sea ISV originated from the weathering of mica or illite. This detrital origin of diagenetically non-changed ISV is supported by the unusual distribution of layer types in these minerals: I, S, and V layers have a significant tendency to segregation (Drits et al. 1997). In addition, the ISV is associated with mixed-layer kaolinite-illite-vermiculite, which also probably formed through the weathering of illites (Drits et al. 1997). The dominating tv layers in these ISV determined in the present work is in agreement with the

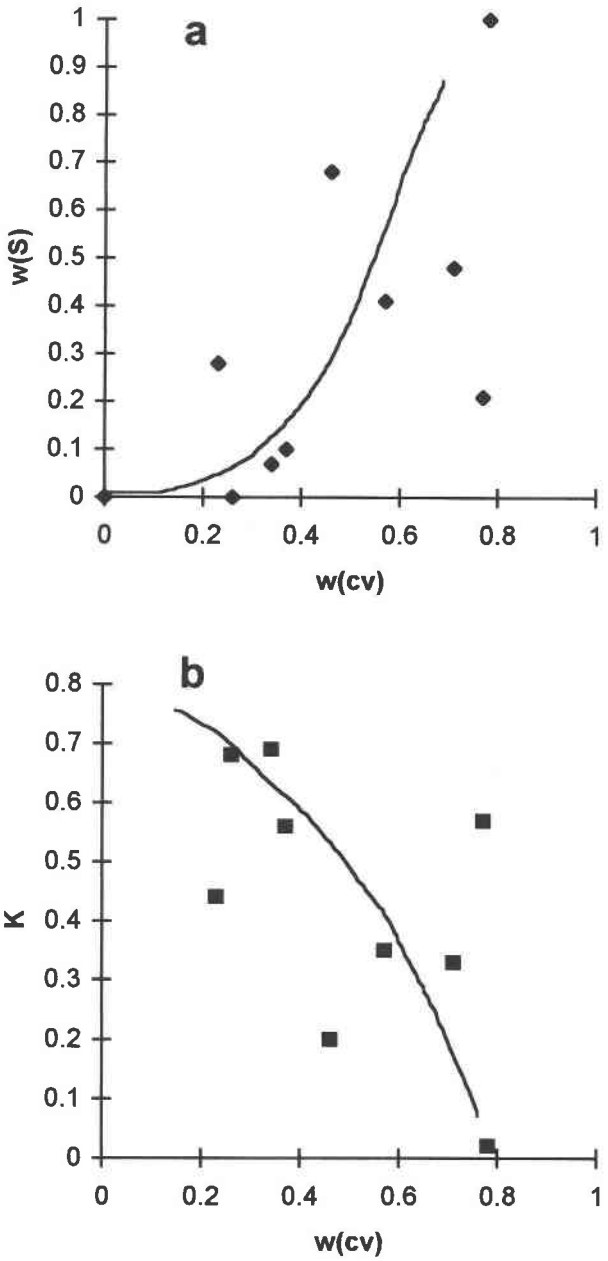

FIGURE 9. The dependence between w_{cv} determined by EWA and w_s (**a**) and the content of fixed K per $O_{10}(OH)_2$ (**b**).

origin of these minerals as well as with the results of Deconinck and Chamley (1995). Furthermore, the proportion of cv and tv layers in the North Sea shale ISV does not change during diagenesis, supporting the conclusion of Drits et al. (1997) that the reaction in these ISV is a solid-state transformation. Thus, determination of tv and cv layer contents in I/S and ISV may provide additional information concerning origin as well as structural mechanism of transformation of these minerals.

Acknowledgments

V.A. Drits, H. Lindgreen, and A. Salyn are grateful to NATO for the Linkage Grant HTECH.LG without which this investigation would not have been possible. V.A. Drits and A. Salyn are grateful to the Russian Science Foundation for financial support. We are grateful to V. Šucha for samples from Doluá Ves and to reviewers R. C. Reynolds and S. Hillier for improving the manuscript.

References cited

Ahn, J.H. and Peacor, D.R. (1986a) Transmission and analytical electron microscopy of the smectite-to-illite transition. Clays and Clay Minerals, 34, 165–179.

———(1986b) Transmission electron microscope data for rectorite: Implications for the origin and structure of "fundamental particles". Clays and Clay Minerals, 34, 180–186.

———(1989) Illite-smectite from Gulf Coast shales: A reappraisal of transmission electron microscope images. Clays and Clay Minerals, 37, 542–546.

Ahn, J.H. and Buseck, P.R. (1990) Layer-stacking sequences and structural disorder in mixed-layer illite/smectite: Image simulations and HRTEM imaging. American Mineralogist, 75, 267–275.

Bell, T.E. (1986) Microstructure in mixed-layer illite/smectite and its relationship to the reaction of smectite to illite. Clays and Clay Minerals, 34, 146–154.

Bethke, C.M. and Altaner, S.P. (1986) Layer-by-layer mechanism of smectite illitization and application of a new rate law. Clays and Clay Minerals, 34, 136–145.

Burst, J.F. (1969) Diagenesis of Gulf Coast clayey sediments and its possible relation to petroleum migration. American Association of Petroleum Geologists Bulletin, 53, 73–93.

Deconinck, J.F. and Chamley, H. (1995) Diversity of smectite origins in Late Cretaceous sediments: Examples of chalks from Northern France. Clay Minerals, 30, 356–379.

Drits, V.A. (1987) Mixed-layer minerals: Diffraction methods and structural features. In L.G. Schultz, H. van Olphen, and F.A. Mumpton, Eds., Proceedings of the International Clay Conference, Denver, 1985, p. 33–45. Clay Minerals Society, Bloomington, Indiana.

Drits, V.A. and Sakharov, B.A. (1976) X-ray Analysis of Mixed-layer Clay Minerals. Nauka, Moscow, 256 p. (in Russian).

Drits, V.A. and McCarty, D.K. (1996) The nature of diffraction effects from illite and illite-smectite consisting of interstratified trans-vacant and cis-vacant 2:1 layers: A semiquantitative technique for determination of layer-type content. American Mineralogist, 81, 852–863.

Drits, V.A., Plançon, A., Sakharov, B.A., Besson, G., Tsipursky, S.I., and Tchoubar, C. (1984) Diffraction effects calculated for structural models of K-saturated montmorillonite containing different types of defects. Clay Minerals, 19, 541–562.

Drits, V.A., Weber, F., Salyn, A.L., and Tsipursky, S.L. (1993) X-ray identification of one-layer illite varieties: Application to the study of illites around uranium deposits of Canada. Clays and Clay Minerals, 41, 389–398.

Drits, V.A., Besson, G., and Muller, F. (1995) An improved model for structural transformations of heat-treated aluminous dioctahedral 2:1 layer silicates. Clays and Clay minerals, 43, 718–731.

Drits, V.A., Salyn, A.L., and Šucha, V. (1996) Structural transformation of interstratified illite-smectites from Dolná Ves hydrothermal deposits: Dynamics and mechanisms. Clays and Clay Minerals, 44, 181–190.

Drits, V.A., Sakharov, B.A., Lindgreen, H., and Salyn, A. (1997) Sequential structure transformation of illite-smectite-vermiculite during diagenesis of Upper Jurassic shales from the North Sea and Denmark. Clay Minerals, 32, 351–371.

Eberl, D.D. (1993) Three zones of illite formation during burial diagenesis and metamorphism. Clays and Clay Minerals, 41, 26–37.

Grim, R.E. (1968) Clay Mineralogy. In F. Press, Ed., International Series in the Earth and Planetary Sciences, 596 p. McGraw-Hill Book company, London.

Guggenheim, S. (1990) The dynamics of thermal decomposition in aluminous dioctahedral 2:1 layer silicates: A crystal chemical model. In V.C. Farmer and Y. Tardy, Eds., Proceedings of the International Clay Conference, p. 99–107. Strasbourg, France.

Guthrie, G.D. and Veblen, D.R. (1989) High-resolution transmission electron microscopy of mixed-layer illite/smectite: Computer simulations. Clays and Clay Minerals, 37, 1–11.

Hansen, P.L. and Lindgreen, H. (1987) Structural investigations of mixed-layer smectite-illite clay minerals from North Sea oil source rocks. In G.W. Bailey, Ed., Proceedings of the 45th Annual Meeting of the Electron Microscopy Society of America, p. 374–375. San Francisco Press, San Francisco.

———(1989) Mixed-layer illite/smectite diagenesis in Upper Jurassic claystones from the North Sea and onshore Denmark. Clay Minerals, 24, 197–213.

Hower, J., Eslinger, E.V., Hower, M.E., and Perry, E.A. (1976) Mechanism of burial methamorphism of argillaceous sediment: I. Mineralogical and chemical evidence. Geological Society of America Bulletin, 87, 725–737.

Inoue, A. and Kitagawa, R. (1994) Morphological characteristics of illitic clay minerals from a hydrothermal system. American Mineralogist, 79, 700–711.

Inoue, A., Kohyama, N., Kitagawa, R., and Watanabe, T. (1987) Chemical and morphological evidence for the conversion of smectite to illite. Clays and Clay Minerals, 35, 111–120.

Inoue, A., Velde, B., Meunier, A., and Touchard, G. (1988) Mechanism of illite formation during smectite-to-illite conversion in a hydrothermal system. American Mineralogist, 73, 1325–1334.

Klimentidis, R.D. and Mackinnon, I.D.R. (1986) High-resolution imaging of ordered mixed-layer clays. Clays and Clay Minerals, 34, 155–164.

Lanson, B. and Champion, D. (1991) The I/S-to-illite reaction in the late stage diagenesis. American Journal of Science, 291, 473–506.

Lindgreen, H. (1991) Elemental and structural changes in illite/smectite mixed-layer clay minerals during diagenesis in Kimmeridgian-Volgian (-Ryazanian) clays in the Central Trough, North Sea and the Norwegian-Danish Basin. Bulletin of the Geological Society of Denmark, 39, 1–82.

Lindgreen, H. and Hansen, P.L. (1991) Ordering of illite-smectite in Upper Jurassic claystones from the North Sea. Clay Minerals, 26, 105–125.

Lindgreen, H., Garnaes, J., Besenbacher, F., Laegsgaard, E., and Stensgaard, I. (1992) Illite-smectite from the North Sea investigated by scanning tunnelling microscopy. Clay Minerals, 27, 331–342.

Mackenzie, R.C. (1957) The Differential Thermal Investigation of Clays. Mineralogical Society, London, 456 p.

McCarty, D. and Reynolds, R.C. (1995) Rotationally disordered illite/smectite in Paleozoic K-bentonites. Clays and Clay Minerals, 43, 271–283.

Morgan, D.J. (1977) Simultaneous DTA-EGA of minerals and natural mineral admixtures. Journal of Thermal Analysis, 12, 245–263.

Nadeau, P.H. and Bain, D.C. (1986) Composition of some smectites and diagenetic illitic clays and implications for their origin. Clays and Clay Minerals, 34, 455–464.

Nadeau, P.H., Tait, M.J., McHardy, W.J., and Wilson, M.J. (1984) Interstratified XRD characteristics of physical mixtures of elementary clay particles. Clay Minerals, 19, 67–76.

Nadeau, P.H., Wilson, M.J., McHardy, W.J., and Tait, J.M. (1985) The conversion of smectite to illite during diagenesis: evidence from some illitic clays from bentonites and sandstones. Mineralogical Magazine, 49, 393–400.

Pevear, D.R., Williams, V.E., and Mustoe, G.E. (1980) Kaolinite, smectite,

and K-rectorite in bentonites: Relation to coal rank in Tulameen, British Colombia: Clays and Clay Minerals, 28, 241–254.

Reynolds, R.C. (1980) Interstratified clay minerals. In G.W. Brindley and G. Brown, Eds., Crystal structures of clay minerals and their X-ray identification, p. 249–303. Mineralogical Society, London.

———(1985) NEWMOD, a computer program for the calculation of one-dimensional diffraction patterns of mixed-layered clays. R.C. Reynolds, Hanover, New Hampshire.

———(1993) Three-dimensional powder X-ray diffraction from disordered illite: Simulation and interpretation of the diffraction patterns. In R.C. Reynolds and J.R. Walker, Eds., Clay Minerals Society Workshop Lectures, Vol. 5: Computer Applications to X-ray Powder Diffraction Analysis of Clay Minerals, p. 43–77. The Clay Minerals Society, Boulder, Colorado.

Shutov, V.D., Drits, V.A., and Sakharov, B.A. (1969) On the mechanism of postsedimentary transformations of montmorillonite into hydromica. In Proceedings of the International Clay Conference, Tokyo, 1, 523–532, Jerusalem, Israel.

Środoń, J. (1980) Precise identification of illite-smectite interstratifications by X-ray powder diffraction. Clays and Clay Minerals, 28, 401–411.

———(1984) X-ray powder diffraction identification of illitic materials. Clays and Clay Minerals, 32, 337–349.

Środoń, J., Elsass, F., McHardy, W.J., and Morgan, D.J. (1992) Chemistry of illite-smectite inferred from TEM measurements of fundamental particles. Clay Minerals, 27, 137–158.

Šucha, V., Kraus, I., Mosser, C., Hroncova, Z., and Siranova, V. (1992) Mixed-layer illite/smectite from the Dovna Ves hydrothermal deposit, the Western Carpathians Kremnica MTS. Bratislava: Geologia Carpatica, Clays, series 1, 13–21.

Šucha, V., Środoń, J., Elsass, F., and McHardy, W.J. (1996) Particle shape versus coherent scattering domain of illite/smectite: evidence from HRTEM of Dolná Ves clays. Clays and Clay Minerals, 44, 665–671.

Tsipursky, S.I. and Drits, V.A. (1984) The distribution of octahedral cations in the 2:1 layers of dioctahedral smectites studied by oblique-texture electron diffraction. Clay Minerals, 19, 177–193.

Veblen, D.R., Guthrie, G.D., Livi, K.J.T., and Reynolds, R.C. (1990) High-resolution transmission electron microscopy and electron diffraction of mixed-layer illite-smectite: Experimental results. Clays and Clay Minerals, 38, 1–13.

Ylagan, R.F. (1996) Mineralogy and geochemistry associated with hydrothermal alteration of a rhyolitic hyaloclastite from Ponza Island, Italy, 152 p. Dissertation, University of Illinois at Urbana-Champaign.

Ylagan, R.F., Altaner, S.P., and Pozzuoli, A. (1996) Hydrothermal alteration of a rhyolitic hyaloclastite from Ponza Island, Italy. Journal of Vulcanology and Geothermal Research, 74, 215–231.

Manuscript received October 14, 1997
Manuscript accepted June 21, 1998
Paper handled by Simon A.T. Redfern